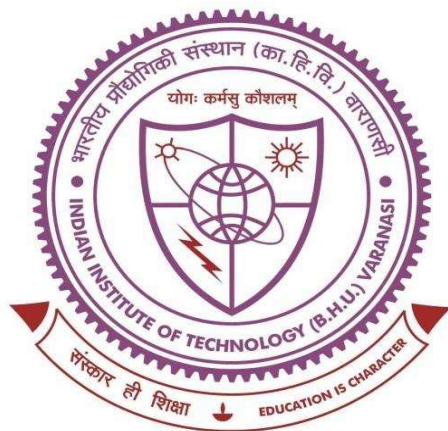


INVESTIGATIONS ON NICKELATE BASED SYSTEM AS AIR-ELECTRODES FOR FUEL CELL APPLICATIONS



THESIS SUBMITTED FOR THE AWARD OF THE DEGREE OF

Doctor of Philosophy

In

Physics

By

Manisha Chauhan

Under the supervision of

Prof. Prabhakar Singh

DEPARTMENT OF PHYSICS
INDIAN INSTITUTE OF TECHNOLOGY
BANARAS HINDU UNIVERSITY
VARANASI-221005
INDIA

17171014

2022

Dedicated
To
my beloved Family
and my Preceptor

CERTIFICATE

It is certified that the work contained in the thesis titled “**INVESTIGATIONS ON NICKELATE BASED SYSTEM AS AIR-ELECTRODES FOR FUEL CELL APPLICATIONS**” by “**MANISHA CHAUHAN**” (Roll No. **17171014**), in partial fulfillment of the requirement for the award of the degree of **Doctor of Philosophy** at **Indian Institute of Technology (B.H.U), Varanasi** is a record of her own work carried out under my supervision and guidance and this work has not been submitted elsewhere for a degree.

It is further certified that the student has fulfilled all the requirements of Comprehensive Examination, Candidacy, and SOTA for the award of Ph.D. Degree.

Date:

Place: Varanasi

Supervisor

(Prof. Prabhakar Singh)

DECLARATION BY THE CANDIDATE

I, **MANISHA CHAUHAN** (Roll No. 17171014), certify that the work embodied in this thesis is my own bonafide work and carried out by me under the supervision of **PROF. PRABHAKAR SINGH** from **JULY, 2017** to **SEPTEMBER 2022** at the **DEPARTMENT OF PHYSICS**, Indian Institute of Technology, Varanasi. The matter embodied in this thesis has not been submitted for the award of any other degree/diploma. I declare that I have faithfully acknowledged and given credits to the research workers wherever their works have been cited in my work in this thesis. I further declare that I have not willfully copied from any other's work, paragraphs, text, data, results, *etc.*, reported in journals, books, magazines, reports dissertations, theses, *etc.*, or available on websites and have not included them in this thesis and have not cited as my own work.

Date:

Place: Varanasi

Signature of the Student

(MANISHA CHAUHAN)

CERTIFICATE BY THE SUPERVISOR

It is certified that the above statement made by the student is correct to the best of our knowledge.

Supervisor

(Prof. Prabhakar Singh)

Signature of Head of Department

COPYRIGHT TRANSFER CERTIFICATE

Title of the Thesis: “Investigations on Nickelate based system as air-electrodes for fuel cell applications”

Name of the Student: Manisha Chauhan

Copyright Transfer

The undersigned hereby assigns to the Indian Institute of Technology (Banaras Hindu University) Varanasi all rights under copyright that may exist in and for the above thesis submitted for the award of the “*Doctor of Philosophy*”.

Date:

Signature of the Student

Place: **IIT (BHU), Varanasi**

(MANISHA CHAUHAN)

Note: However, the author may reproduce or authorize others to reproduce material extracted verbatim from the thesis or derivative of the thesis for author's personal use provided that the source and the Institute's copyright notice are indicated.

Acknowledgments

“The journey of thousands of miles, begins with a single step.”

As they say, "Hard effort overcomes all," but not fully. My efforts are reflected in this thesis. Nevertheless, it also features contributions from other individuals who supported me while I was a student at the Indian Institute of Technology (Banaras Hindu University), Varanasi. It would make me very happy to thank everyone who supported me throughout the ups and downs of my time as a Ph.D. scholar in the lines that follow.

First and foremost, I would like to express my sincere gratitude to my supervisor Prof. Prabhakar Singh, department of physics at the Indian Institute of Technology (Banaras Hindu University), who oversaw my thesis and provided me with guidance, motivation, and encouragement as I pursued my scientific interest. I will always remember your encouraging approach to developing my own personality. Being in his company has been both a privilege and a joy.

In addition, I would like to extend my sincere gratitude to RPEC members Prof. Sandip Chatterjee, Department of Physics, Indian Institute of Technology (Banaras Hindu University), and Prof. Ashutosh K. Dubey, Department of Ceramic Engineering, Indian Institute of Technology (Banaras Hindu University), for their insightful comments and suggestions, without which this work would not have been finished.

Additionally, I would like to express my sincere gratitude to all of the department's professors all faculty members for their kind support at all moment during the progress of my research., I thank the department's office workers in general as well as the administrators at IIT (BHU) for their assistance and cooperation during my stay.

I want to express my gratitude to Dr. Pardeep K. Jha and Dr. Priyanka A. Jha of the Physics Department at IIT (BHU), Varanasi, for their insightful advice and scientific viewpoints that helped me overcome several obstacles during my research.

A special thanks to Dr. Ajay Shankar Bangwal, my senior and friend, for his important contribution to my thesis in the form of perceptive recommendations and discussion. I really appreciate your support and value the contribution you made.

My seniors, Dr. Raghvendra Pandey, Dr. Bheeshma Pratap Singh, Dr. Vani Pawar, Dr. P. K. Dubey, Dr. Pravin Kumar, Dr. Onkar Nath Verma, Mr. Ashish Yadav, Dr. Manish Kumar, Dr. Pragati Singh, and Dr. Vandna Tomar, deserve my deepest gratitude for their assistance. I'm going to miss our conversations a lot. Additionally, I thank Mr. Prem Chand Bharti, Ms. Uma Sharma, Mr. Ashish Kumar Ranjan, Ms. Kamana, Ms. Manisha Sharma, Ms. Swarnima Singh, Mr. Jay Narayan Mishra, Ms. Gargi, and Mr. Vishal Singh for being my lab partners. Thank you to everybody. You always made working in the lab so enjoyable for me.

Then there are all the friends I've made on campus; because of their companionship, I was able to enjoy my time at IIT(BHU). I'll always remember my time spent with Mr. Suraj Yadav, Ms. Srishti Paliwal, and Ms. Jyoti Sharma. Other than this, I would want to thank my persistent friends Dr. Iram Saifi, Mr. Krishna Bijalwan, Ms. Chinki Malik, Mrs. Ankita Dimri, Ms. Ankita Jayara, and Mr. Nihar Kathpalia for making my journey so lovely with their encouragement and well wishes. I want to thank everyone for making my life enjoyable, joyful, and festive.

I am forever indebted to my beloved Grand Mother Mrs. Krishna Devi, My father, Dr. Girendra Kumar Chauhan, and my mother, Mrs. Sushma Devi, for their inseparable support and prayers. I have a huge gratitude for my parents, who helped to shape my perspective and taught me the values that are important in life. I am appreciative of my brother Mr. Abhishek Chauhan's continued support and belief in me. I genuinely hope that my family will be proud of me for this thesis. I feel deep gratitude for my parents, who formed a part of my vision and taught me the good things that matter in life. I sincerely hope this thesis makes my family feel proud of me.

The assistance of INSPIRE, DST(INDIA) has been acknowledged in due course. I would like to sincerely thank CIFC, IIT (BHU), Varanasi for their assistance in carrying out the characterization of the synthesized samples.

I also want to thank everyone who helped me, directly or indirectly, in finishing this enormous task but was too numerous to mention individually.

Last but not least, I give thanks to the Almighty for being so kind as to grant me the perseverance and wisdom necessary to finish this research study. I dedicated my work to Mahadev, the universe's creator, who has been by my side the entire time I've been pursuing my Ph.D. and living my life.

Date:

Place: Varanasi

(Manisha Chauhan)

Contents

CERTIFICATE.....	i
DECLARATION BY THE CANDIDATE	iii
COPYRIGHT TRANSFER CERTIFICATE.....	v
Acknowledgments.....	vii
Contents	xi
LIST OF FIGURES	xv
LIST OF TABLES.....	xxv
LIST OF SYMBOLS AND ABBREVIATIONS.....	xxvii
PREFACE.....	xxix
CHAPTER 1: Introduction and Literature Review	1
1.1 Overview.....	1
1.2 Fuel Cells Basics	3
1.2.1 History of Fuel Cell:.....	4
1.2.2 Working principle of the f Fuel cell	5
1.2.3 Types of Fuel cells.....	8
1.3 Solid Oxide Fuel Cell (SOFC)	9
1.3.1 The basic operation of SOFC	10
1.3.2 Components of SOFC.....	12
1.4 Reaction and Kinetic mechanism for the air electrode.....	16
1.4.1 Mechanism of Oxygen Reduction Reaction (ORR)	17
1.4.2 Mechanism for Oxygen Evolution Reaction (OER)	21
1.5 Electrodes for fuel Cells: An Overview	24
1.5.1 Magnetite based cathodes	24
1.5.2 Ferrite based cathodes.....	25
1.5.3 Cobaltite based cathode.....	26
1.5.4 Ferro-cobaltite based cathode	27
1.5.5 Nickelate based cathodes.....	28
1.6 State of the Art: Nickelate based cathode	28

1.6.1	Perovskite structure.....	29
1.6.2	Ruddlesden-popper type oxide:.....	30
1.7	Layered $\text{Ln}_2\text{NiO}_{4+\delta}$ nickelates:	31
1.7.1	Overview of $\text{Sm}_{2-x}\text{Sr}_x\text{NiO}_{4-\delta}$	35
1.8	The objective of the Present Research Work	36
CHAPTER 2: Materials and Methods		41
2.1	Overview	41
2.2	Specification of the Materials used	41
2.3	Synthesis of Materials.....	42
2.3.1	Solid-state reaction route (SSR)	42
2.3.2	Sol Gel Method	44
2.3.3	Spin Coating Technique:	45
2.3.4	Pulse Laser Deposition Technique (PLD).....	46
2.4	Characterization Techniques	48
2.4.1	Thermogravimetric Analysis (TGA)	48
2.4.2	Differential Scanning Calorimetry (DSC)	49
2.4.3	Bench-Top X-Ray Diffraction (BT-XRD).....	51
2.4.4	Fourier-Transform Infrared Spectroscopy (FTIR).....	53
2.4.5	Scanning Electron Microscopy (SEM)	55
2.4.6	Atomic Force Microscopy (AFM).....	57
2.4.7	X-ray Photoelectron Spectroscopy (XPS)	59
2.4.8	Cyclic Voltammetry (CV)	61
2.4.9	Density Measurement.....	63
2.5	Methods and Analysis.....	64
2.5.1	Rietveld Refinement Technique.....	64
2.5.2	Software for Analyzing the Obtained Data	67
CHAPTER 3: Oxygen reduction reaction in a Ruddlesden-Popper perovskite $\text{SmSrNiO}_{4-\delta}$.....		71
3.1	Introduction	71
3.2	Methodology.....	73
3.2.1	Sample preparation	73
3.2.2	Characterization techniques	73
3.3	Result and discussion.....	74

3.3.1	Structural details of the calcined powder	74
3.3.2	Structural Variation after CV	89
3.4	Conclusion	96
CHAPTER 4: Electrocatalytic behaviour for $\text{Sm}_{2-x}\text{Sr}_x\text{NiO}_{4-6}$ ($x = 0.4$ to 1.0) Ruddlesden Popper based systems		99
4.1	Introduction.....	99
4.2	Experimental Procedure.....	102
4.2.1	Synthesis Technique	102
4.2.2	Characterization techniques.....	103
4.3	Results and Discussion	104
4.3.1	Structural and electrical Studies.....	104
4.3.2	Thermogravimetric studies	111
4.3.3	Microstructural Studies	112
4.3.4	Catalysis Studies	113
4.4	Conclusion	133
CHAPTER 5: Electrochemical performance of A-site substituted SmSrNiO_{4-6} for energy storage applications.....		137
5.1	Introduction.....	137
5.2	Methods and Materials	139
5.2.1	Synthesis Technique	139
5.2.2	Characterization Techniques	140
5.3	Results and Discussion	140
5.3.1	Thermogravimetry analysis	140
5.3.2	Structural and microstructural studies.....	142
5.3.3	Electrochemical properties	147
5.3.4	Electronic Studies	155
5.3.5	Conclusion	160
CHAPTER 6: Electrocatalytic activity of nickel oxide thin film:		163
6.1	Introduction.....	163
6.2	Synthesis and characterization of electrocatalyst.....	165
6.3	Results and Discussion	166
6.3.1	Structural Studies	166

6.3.2	AFM and SEM studies	167
6.3.3	FTIR analysis.....	169
6.3.4	Electrocatalytic Studies	169
6.4	Conclusion.....	179
	CHAPTER 7: Conclusions and Future Scopes	183
7.1	Conclusion of the Present Investigation	183
7.2	Scope for Future Work.....	186
	References	187
	List of Publications	209

LIST OF FIGURES

		Page No.
Chapter I	Introduction and Literature review	
Fig. 1.1	Worldwide consumption forecast till 2050	3
Fig. 1.2	Schematic diagram of Proton conducting fuel cell	6
Fig. 1.3	Maximum efficiency of hydrogen fuel cell with the steam produced compared to Carnot limit with 50 °C exhaust temperature	7
Fig. 1.4	Schematic diagram of (a) oxygen-ion and (b) proton conduction in a solid oxide fuel cell	11
Fig. 1.5	Schematic representation of Triple Phase Boundary	17
Fig. 1.6	Schematic illustration of three reaction paths for the cathodic reaction	19
Fig. 1.7	Number of publications in the last 5 years the for the keyword of cathode materials	29
Fig. 1.8	Atomic structure in mixed conducting perovskite, left image represents ions' position in a cubic structure, and right image represents the BO ₆ octahedra with oxygen vacancy migration path	30
Fig. 1.9	Crystal structures of A ₂ BO ₄ phases (A = Ln and B = Ni)	32
Fig. 1.10	(a) The unit cell of the ideal perovskite structure, building block of ideal tetragonal K ₂ NiF ₄ -structure. (b) The unit cell of K ₂ NiF ₄ along the (a, b)-directions (c) Two-dimensional	33

	character of the K_2NiF_4 structure. Unit cells are outlined in yellow	
Chapter II	Materials and Methods	
Fig. 2.1	Schematic diagram of solid-state route (SSR) method	43
Fig. 2.2	Schematic diagram of sol gel method	45
Fig. 2.3	(a) Spin coating system used in present work (b) schematic diagram of thin film formation by spin coating technique	46
Fig. 2.4	Schematic diagram of pulse laser deposition technique	47
Fig. 2.5	(a) Schematic diagram of TGA (b) Experimental setup of TGA at Central instrument facility (CIF) IIT (BHU)	49
Fig. 2.6	Experimental setup of DSC at Central instrument facility (CIF) IIT (BHU)	50
Fig. 2.7	(a) Interpretation of Bragg's law in 2-dimensional crystal lattice (b) Experimental setup of BT-XRD at Central instrumentation facility CIF IIT(BHU)	52
Fig. 2.8	Schematic diagram of Working Principle of FTIR (b) Experimental setup of FTIR at the central instrumentation facility CIF IIT(BHU)	54
Fig. 2.9	(a) Operating Principle of SEM (b) Experimental setup of SEM at central instrumentation facility CIF IIT(BHU)	56
Fig. 2.10	(a) Block diagram and (b) experimental set up of AFM.	58
Fig. 2.11	Basic component of monochromatic XPS system	60
Fig. 2.12	(a) cyclic voltammogram (b) Experimental set up of Cyclic voltammetry	62

Fig. 2.13	Density measurement kit by Sartorius, BSA2245-CW	64
Chapter III	Oxygen reduction reaction in a Ruddlesden-Popper perovskite (SmSr)NiO_{4-δ}	
Fig. 3.1	(a) TGA, DTGA of raw powder and (b) XRD of calcined powder SmSrNiO _{4-δ}	75
Fig. 3.2	(a) XRD pattern of the SmSrNiO _{4-δ} sample sintered at different sintering temperatures 1250 °C, 1300 °C, 1350 °C, 1400 °C, and 1425 °C, (b) Shifting and FWHM of the studied samples corresponding to 2θ ~ 32°, (c) Shifting and FWHM of the studied samples corresponding to 2θ ~ 24°, (d) Diffuseness of XRD peak (011) corresponding to 2θ ~ 24°	76
Fig. 3.3	(a) X-ray diffractograms of the SmSrNiO _{4-δ} sample sintered at different sintering temperatures 1250 °C, 1300 °C, 1350 °C, 1400 °C, and 1425 °C corresponding to 2θ ~ 43° - 46°, (b) Phase purity of the studied samples (c) Variation of lattice parameters with the sintering temperature	77
Fig. 3.4	Rietveld refined X-ray diffractograms of the SmSrNiO _{4-δ} sample sintered at different sintering temperatures 1250 °C, 1300 °C, 1350 °C, 1400 °C, and 1425 °C. The figure contains the data points, intensity obtained, difference profiles and Bragg positions of the samples sintered at different temperatures	79
Fig. 3.5.	Variation of density with the increase in sintering temperature showing a hump at 1400 °C, proving the optimized sintering temperature	81

Fig. 3.6	(a-e) SEM micrographs of SmSrNiO _{4-δ} sample sintered at different sintering temperatures (e) inset surface of the sample sintered at 1425 °C and (f) Excess Ni measured through EDX of the studied samples	81
Fig. 3.7	(a) Rietveld refinement of X-ray diffractograms of SmSrNiO _{4-δ} sample sintered at sintering temperatures 1250 °C and 1425 °C, respectively, (b) structure obtained from Diamond software using cif files from Rietveld refinement (c) Transient current response along with the exponential fit for the time constant of the sample sintered at sintering temperatures 1250 °C and 1425 °C, respectively	82
Fig. 3.8	TGA of SmSrNiO _{4-δ} sample sintered at sintering temperatures 1250 °C and 1425 °C in N ₂ and O ₂ atmospheres, respectively	84
Fig. 3.9	The dm/dT values of the (SmSr)NiO _{4-δ} samples sintered at 1250 °C and 1425 °C under N ₂ and O ₂ atmospheres	86
Fig. 3.10	(a) Cyclic Voltammetry and (b, c) SEM of (SmSr)NiO _{4-δ} sample sintered at 1250 °C and 1425 °C, respectively	87
Fig. 3.11	Tafel plot showing E _{corr} , I _{corr} , and Corrosion rate (CR) of the samples sintered at 1250 °C and 1425 °C (here corrosion rate in mmY stands for mm/year)	89
Fig. 3.12	(a) The different oxides band formations, hydroxyl band groups, are studied through FTIR transmission spectra of SmSrNiO _{4-δ} sample sintered at different sintering temperatures (b) FTIR spectra in the range of 400 -700 cm ⁻¹ for SmSrNiO _{4-δ} sample sintered at different sintering temperatures	91

Fig. 3.13	Rietveld refined X-ray diffractograms of the SmSrNiO _{4-δ} sample sintered at 1250 °C and 1425 °C after cyclic voltammetry	91
Fig. 3.14	A Pre and post effects of CV on the structures of the materials according to the (a) XRD and (b) FTIR of (SmSr)NiO _{4-δ} sample sintered at 1250 °C and 1425 °C, respectively	93
Fig. 3.15	(a) Labels of atoms (b) Structure of (SmSr)NiO _{4-δ} showing the vacant apical oxygens (□) (c) SEM micrographs of porous and pore free samples (d) Surface adsorption mechanism with 4 step and 2 step pathways (e) corresponding alteration in NiO ₆ octahedra	94
Chapter IV	Electrocatalytic behaviour for Sm_{2-x}Sr_xNiO_{4-δ} (x = 0.4 to 1.0) Ruddlesden Popper based system	
Fig. 4.1	depicts the X-ray diffractograms of the sintered pellets of Sm _{2-x} Sr _x NiO _{4-δ} (x = 0.4-1.0 at the steps of 0.2) samples (Right panel) shows the formation of secondary phase	105
Fig. 4.2	depicts the X-ray diffractograms of the sintered pellets of Sm _{2-x} Sr _x NiO _{4-δ} (x = 0.0 and 0.2)	106
Fig. 4.3	(a) Variation of microstrain and phase purity with x for the studied samples Sm _{2-x} Sr _x NiO _{4-δ} (x = 0.4-1.0 at the steps of 0.2). (b) Lattice parameters obtained from Rietveld refinement of the X-ray diffractograms	107
Fig. 4.4	(a) Rietveld refinement of the X-ray diffractograms of the studied samples Sm _{2-x} Sr _x NiO _{4-δ} (x = 0.4 - 1 at the steps of 0.2). It is seen from the goodness of fit factor χ^2 that x = 0.4 and 0.6 show orthorhombic Fmmm symmetry and x = 0.8, 1.0 showed tetragonal I4/mmm symmetry (b) splitting observed at $2\theta \sim 45^\circ$ confirming the phase change (c) Tetragonal Structure of	109

	SmSrNiO _{4-δ} (d) Variation of Ni, O and ratio of Ni/(Sm+Sr) with x suggesting the compensation mechanism (e) Value of conductivity at 100 °C of bulk Sm _{2-x} Sr _x NiO _{4-δ} ;(e, inset) black coloration on heat treatment.	
Fig. 4.5	(a, b, c, and d) Variation of mass with temperature of the studied samples Sm _{2-x} Sr _x NiO _{4-δ} (x = 0.4 - 1 at the steps of 0.2). It is seen that structural change is governed with the oxygen non-stoichiometry (e, f, g, and h) dm/dT curves with temperature of the studied samples Sm _{2-x} Sr _x NiO _{4-δ} (x = 0.4 - 1 at the steps of 0.2), the position of kinks and peaks are in accordance with the mass loss curves	112
Fig. 4.6	SEM micrographs and their respective insets depict the grain size histograms for the Sm _{2-x} Sr _x NiO _{4-δ} (x = 0.4 – 1.0 at the steps of 0.2)	113
Fig. 4.7	(a) represents the cyclic voltammograms showing ECE mechanism with the scan rate for x = 0.6 and ETC mechanism with the 4-electron process for x =1.0 (b) Variation of area with the scan rate for x = 0.6 and 1.0 (c) RS equation plot between the current density and \sqrt{v} for x = 0.6 and 1.0 (d) log-log plot of current density and v for the studied samples	115
Fig. 4.8	Cyclic Voltammograms with the scan rate of the Sm _{2-x} Sr _x NiO _{4-δ} (x = 0.4)	115
Fig. 4.9	Cyclic Voltammograms with the scan rate of the Sm _{2-x} Sr _x NiO _{4-δ} (x = 0.8)	116
Fig. 4.10	First and second order derivative CV curves showing E _{p/2} (black dash lines) and E _i (red dash lines) of the studied samples for 30 mV/sec and 250 mV/sec for the estimation of parameters	117

Fig. 4.11	Variation of $E_{p/2}$ and E_i with the scan rate for the forward scans of $x = 0.6$ and 1.0	118
Fig. 4.12	SEM micrographs and respective grain size histograms for the thin films of $Sm_{2-x}Sr_xNiO_{4-\delta}$ ($x = 0.6, 1.0$ thin film)	119
Fig. 4.13	X-ray diffractograms of the films of $Sm_{2-x}Sr_xNiO_{4-\delta}$ ($x = 0.6$ and $x = 1$) samples	120
Fig. 4.14	a) represents the cyclic voltammograms with the scan rate for $x = 0.6$ and $x = 1.0$ thin films (b) Variation of area with the scan rate for $x = 0.6$ and 1.0 thin films (c) RS equation plot between the current density and \sqrt{v} for $x = 0.6$ and 1.0 thin films (d) log-log plot of current density and v for the studied thin films	121
Fig. 4.15	First and second order derivative CV curves for $x = 0.6$ and 1.0 thin films at 30 mV/sec and 250 mV/sec for the estimation of parameters $E_{p/2}$ and E_i	122
Fig. 4.16	shows the variation of $E_{p/2}$ and E_i with the scan rate for the forward scans of $x = 0.6$ and 1.0 thin films	123
Fig. 4.17	Tafel plot showing E vs $Ag/AgCl$ (V) and $\log J$ (mA/cm^2) and the insets a) and b) correspond to the corrosion rates for $x = 0.6$ and 1.0 , respectively	124
Fig. 4.18	Tafel plot showing E vs $Ag/AgCl$ (V) and $\log J$ (mA/cm^2) correspond to the corrosion rates for $x = 0.6$ and 1.0 thin films, respectively	125
Fig. 4.19	(a) Variation of Tafel slope (TS) at CR and transpassive region (TS_{TR}) with composition for bulk $Sm_{2-x}Sr_xNiO_{4-\delta}$ (b) Tafel slope at CR and transpassive region for $Sm_{2-x}Sr_xNiO_{4-\delta}$ ($x =$	126

	0.6 and 1.0) thin films and (c) Mechanism for Oxygen evolution reaction with the variation in Tafel slope	
Fig. 4.20	FTIR spectra of the samples $\text{Sm}_{2-x}\text{Sr}_x\text{NiO}_{4-\delta}$ at $x = 0.6$ and 1.0	129
Fig. 4.21	Deconvoluted XPS spectra using XPS peak 4.1 of Sm3d, Sr 3d, Ni2p and O1s with Shirley background of the samples $\text{Sm}_{2-x}\text{Sr}_x\text{NiO}_{4-\delta}$ at $x = 0.6$ and 1.0	131
Fig. 4.22	Wide XPS spectra of the $\text{Sm}_{2-x}\text{Sr}_x\text{NiO}_{4-\delta}$ ($x = 0.6$ and 1.0)	131
Fig. 4.23	Chronoamperometric response showing transient decay tie for the $x = 0.6$ and 1.0 thin films	132
Chapter V	Electrochemical performance of A-site substituted $\text{SmSrNiO}_{4-\delta}$	
Fig. 5.1	TGA and dm/dT variation of $\text{Sm}_{1-x}\text{La}_x\text{Sr}_{1-x}\text{Ca}_x\text{NiO}_{4-\delta}$ ($x = 0.00, 0.05, 0.10, 0.15, 0.20$)	141
Fig. 5.2	(a) The X-ray diffractograms of the sintered $\text{Sm}_{1-x}\text{La}_x\text{Sr}_{1-x}\text{Ca}_x\text{NiO}_{4-\delta}$ ($x = 0.00, 0.05, 0.10, 0.15, 0.20$)	143
Fig. 5.3	(a) Rietveld refinement of the sintered $\text{Sm}_{1-x}\text{La}_x\text{Sr}_{1-x}\text{Ca}_x\text{NiO}_{4-\delta}$ ($x = 0.00, 0.05, 0.10, 0.15, 0.20$) (b) Lattice Parameters and volume variation of the $\text{Sm}_{1-x}\text{La}_x\text{Sr}_{1-x}\text{Ca}_x\text{NiO}_{4-\delta}$ ($x = 0.00, 0.05, 0.10, 0.15, 0.20$)	143
Fig. 5.4	FTIR spectra of the samples $\text{Sm}_{1-x}\text{La}_x\text{Sr}_{1-x}\text{Ca}_x\text{NiO}_{4-\delta}$ ($x = 0.00, 0.05, 0.10, 0.15, 0.20$)	144
Fig. 5.5	SEM Micrographs and the grain size histogram (inset) for $\text{Sm}_{1-x}\text{La}_x\text{Sr}_{1-x}\text{Ca}_x\text{NiO}_{4-\delta}$ ($x = 0.00, 0.05, 0.10, 0.15, 0.20$)	146

Fig. 5.6	Porosity of $\text{Sm}_{1-x}\text{La}_x\text{Sr}_{1-x}\text{Ca}_x\text{NiO}_{4.8}$ ($x = 0.00, 0.05, 0.10, 0.15, 0.20$)	146
Fig. 5.7	(i) CV curve of all the sample at a scan rate of 30 mV/s (ii) CV curve of all the electrode samples at different scan rates	149
Fig. 5.8	CV curves of $\text{Sm}_{1-x}\text{La}_x\text{Sr}_{1-x}\text{Ca}_x\text{NiO}_{4.8}$ ($x = 0.00, 0.05, 0.10, 0.15, 0.20$) at different scan rates	149
Fig. 5.9	Variation of ΔE_p with compositions for all electrode samples	150
Fig. 5.10	Variation of Specific capacitance with scan rate for all the electrode sample	152
Fig. 5.11	b-value plotted for all the compositions	153
Fig. 5.12	(a) value of C_{dl} for all the electrode samples. (b) Chronoamperometry response of all the samples at 1 V	154
Fig. 5.13	Deconvoluted XPS Spectra using XPS peak 4.1 of Sm3d, Sr3d, La3d, Ca2p, Ni2p, and O1s with Shirley background of the samples $\text{Sm}_{1-x}\text{La}_x\text{Sr}_{1-x}\text{Ca}_x\text{NiO}_{4.8}$ ($x = 0.00, 0.10, \text{ and } 0.20$)	158
Fig. 5.14	XPS wide spectrum of $\text{Sm}_{1-x}\text{La}_x\text{Sr}_{1-x}\text{Ca}_x\text{NiO}_{4.8}$ ($x = 0.00, 0.10, 0.20$)	158
Chapter VI	Electrocatalytic activity of nickel oxide thin film	
Fig. 6.1	X-ray diffraction pattern of NiO thin films	167
Fig. 6.2	(a, b) SEM micrograph of sample N ₂ and N ₆ (c, d) Topographical AFM images of sample N ₂ and N ₆ (e, f) 3D images of AFM of both films (g) EDAX analysis of N ₂ and N ₆ thin films	168

Fig. 6.3	FTIR spectra of N ₂ and N ₆ thin films	169
Fig. 6.4	CV response of Samples N ₂ and N ₆ recorded at the scan rate of 15 mV/sec in 0.5M (a) H ₂ SO ₄ (b) Na ₂ SO ₄ (c) KOH media, respectively	170
Fig. 6.5	Variation of area of voltammograms with the scan rate for N ₂ and N ₆ in 0.5M (a, d) H ₂ SO ₄ (b, e) Na ₂ SO ₄ (c, f) KOH media, respectively	171
Fig. 6.6	Cyclic Voltammetric curves for N ₂ and N ₆ at different scan rates in 0.5M (a, d) H ₂ SO ₄ (b, e) Na ₂ SO ₄ (c, f) KOH media, respectively	172
Fig. 6.7	Peak to peak separation ΔE_p observed at the scan rate 15 mV/sec for N ₂ and N ₆ in 0.5M (a) H ₂ SO ₄ (b) Na ₂ SO ₄ (c) KOH media, respectively	172
Fig. 6.8	Peak Current density observed at the scan rate 15 mV/sec for N ₂ and N ₆ in 0.5M (a) H ₂ SO ₄ (b) Na ₂ SO ₄ (c) KOH media, respectively	173
Fig. 6.9	Variation of j_p vs $v^{1/2}$ as per RS equation for N ₂ and N ₆ sample in 0.5M (a) H ₂ SO ₄ (b) Na ₂ SO ₄ (c) KOH media, respectively	174
Fig. 6.10	Variation of Specific capacitance with scan rate for N ₂ and N ₆ samples in 0.5M (a) H ₂ SO ₄ (b) Na ₂ SO ₄ (c) KOH media, respectively	175
Fig. 6.11	b-value plotted for N ₂ and N ₆ in 0.5M (a) H ₂ SO ₄ (b) Na ₂ SO ₄ (c) KOH media, respectively.	176
Fig. 6.12	Cdl value for N ₂ and N ₆ electrodes in 0.5M (a) H ₂ SO ₄ (b) Na ₂ SO ₄ (c) KOH media, respectively	177

Fig. 6.13	Tafel plots for N ₂ and N ₆ electrodes in 0.5M (a, d) H ₂ SO ₄ (b, e) Na ₂ SO ₄ (c, f) KOH media, respectively. Grey part presents the range where tafel slope is calculated	178
Fig. 6.14	Chronoamperometric response for N ₂ and N ₆ in 0.5M Na ₂ SO ₄ medium	179

LIST OF TABLES

		Page No.
<hr/>		
Chapter I	Introduction and Literature review	
Table 1.1	Comparison of different types of Fuel Cells	9
<hr/>		
Chapter II	Materials and Methods	
Table 2.1	Specifications of the materials used along with their chemical formula, purity, and manufacturer used for the preparation of various samples	42
<hr/>		
Chapter III	Oxygen reduction reaction in a Ruddlesden-Popper perovskite (SmSr)NiO_{4-δ}	
Table 3.1	Atomic positions and R-factors obtained after refinement for the SmSrNiO _{4-δ} samples sintered at different temperature	80
Table 3.2	Oxygen deficiency estimated for SmSrNiO _{4-δ} from TGA in O ₂ and N ₂ atmosphere	83
Table 3.3	Lattice Parameters, atomic positions and Occupancies of SmSrNiO _{4-δ} composition after Cyclic Voltammetry	92
<hr/>		
Chapter IV	Electrocatalytic behaviour for Sm_{2-x}Sr_xNiO_{4-δ} (x = 0.4 to 1.0) Ruddlesden Popper based system	

Table 4.1	Molar ratio of the chemicals used for the synthesis of $\text{Sm}_{2-x}\text{Sr}_x\text{NiO}_{4-\delta}$ ($x = 0.4-1$ at the steps of 0.2)	103
------------------	---	------------

Table 4.2	Atomic positions and R-factors obtained after refinement for the $\text{Sm}_{2-x}\text{Sr}_x\text{NiO}_{4-\delta}$ ($x = 0.4$ to 1.0) samples	110
------------------	--	------------

Table 4.3	A Comparison of lattice mismatch, grain size, and crystallite size for $\text{Sm}_{2-x}\text{Sr}_x\text{NiO}_{4-\delta}$ ($x = 0.6$ and 1.0) bulk and thin films.	120
------------------	--	------------

Table 4.4	A comparative of Tafel Slopes of commercial and well-known electrodes with the present work	128
------------------	---	------------

Chapter V Electrochemical performance of A-site substituted $\text{SmSrNiO}_{4-\delta}$

Table 5.1	Comparison of specific capacitance of several reported electrode with present work	151
------------------	--	------------

LIST OF SYMBOLS AND ABBREVIATIONS

AFC	Alkaline Fuel Cell
PEMFC	Proton Exchange Membrane Fuel Cell
DMFC	Direct Methanol Fuel Cell
PAFC	Phosphoric Acid Fuel Cell
MCFC	Molten Carbonate Fuel Cell
SOFC	Solid Oxide Fuel Cell
ORR	Oxygen Reduction Reaction
TEC	Thermal Expansion Coefficient
RT	Room temperature
ASR	Area Specific Resistance
MIEC	Mixed Ionic-Electronic Conductor
CV	Cyclic Voltammetry
EIS	Electrochemical Impedance Spectroscopy
IDEP	Isotope Exchange Depth Profile
OER	Oxygen Evolution Reaction
HER	Hydrogen Evolution Reaction
IT-SOFC	Intermediate Temperature Solid Oxide Fuel Cell
YSZ	Yttrium Stabilized Zirconia
CGO	Gadolinium Doped Ceria
DSC	Differential Scanning Calorimetry
TGA	Thermogravimetry analysis
XRD	X-ray diffraction
JCPDS	Joint Committee on Powder Diffraction Standards

SEM	Scanning Electron Microscopy
XPS	X-ray Photoelectron Spectroscopy
AFM	Atomic Force Microscopy
ATR	Attenuated Total Reflection
SR	Specular Reflection
FTIR	Fourier-Transform Infrared Spectroscopy
FWHM	Full width at Half Maximum
SSR	Solid State Route
SAED	Selected Area Electron Diffraction
V	Volt
RP	Ruddlesden Popper
TR	Transpassive Region
C_P	Specific Capacitance
C_{dl}	Doble Layer Capacitance
SC	Supercapacitor
RS	Randles–Ševčík
CR	Corrosion Rate
TS	Tafel Slope
RT	Room Temperature
RHE	Reversible Hydrogen Electrode

Preface

Global energy demand is continually rising as a result of ongoing industrial development and population increase, meanwhile the conventional fossil fuels such as oil, coal, natural gases, etc., are exhausting swiftly. Presently, these fossil fuels are the primary fuel source that meets to our current energy needs. However, the availability of fossil fuels in the forthcoming years is of enormous matter of concern. The burning of fossil fuels not only leads to several environmental threats by releasing toxic gases but also restricts the accessibility of traditional energy sources. These detrimental effects on environment enable the global warming. The awareness about the energy crisis and greenhouse gas emission has led to the hunt for alternative routes. In order to find an alternative possibility for alternatives routes, the research is focused into two parts namely, in which one part is focused on the sources that are renewable and ecofriendly while second part is focused on those electrochemical devices which can harvest green and clean energy such as fuel cells.

Electrochemical devices for energy storage play a vital part in the energy dependent world for meeting the situation of rapid diminution of fossil fuels. Electrochemical devices either generate electricity from a chemical reaction (like a battery) or use electrical energy to trigger a chemical reaction (like a catalyst). Among the various available electrochemical devices, fuel cell is highly efficient and holds many diversified pros associated with mobile and stationary power generation including both large scale centralized power production as well as in individual homes and businesses, *etc.*

These days, there are various types of fuel cells accessible in the market. Fuel cells are usually categorized via their electrolyte material. They vary in their power outputs, operating

temperatures, electrical efficiencies, and typical applications. Solid oxide fuel cells (SOFCs) correspond to one of the cleanest and most effective options for the direct conversion of a wide variety of fuels to electricity. For example, SOFCs driven by natural gas are preferably suited for distributed power generation. However, the commercialization of SOFC technologies pivots on advances in materials development to significantly reduce the cost while enhancing performance and durability. One of the crucial hurdles to achieve high-performance SOFC systems is the cathodes for oxygen reduction reaction (ORR), which perform inadequately at low temperatures and degrade over time under operating conditions. Similarly, these investigated cathodes can be used as an electrode in many other electrochemical devices as catalyst for oxygen evolution reaction (OER).

In the present research work, Ruddlesden-Popper perovskite $\text{SmSrNiO}_{4-\delta}$ has been chosen for further investigation. Ruddlesden-Popper perovskites (RP perovskites) have shown electrocatalytic properties along with excellent performance in oxygen-solid oxide fuel cells and hydrogen-solid oxide fuel cells. Their performance is basically attributed to fast surface oxygen exchange property and proton and oxygen transport mechanisms. The microstructural design of electrode materials plays an important role, not only in electron and oxygen ion conduction at the electrolyte-electrode and electrode-air interfaces (ORR), but also on the life time of fuel cells. In this regards, $\text{SmSrNiO}_{4-\delta}$ was synthesized by Solid state route method (SSR) at different optimization temperature. The porous and pore-free sample was synthesized at two different temperature and influence of catalysis on the structure after voltammetry was comprehensively studied. It was found these samples synthesized at two different temperatures that pore-free sample with a higher ionic conductivity and catalytic

activity is suitable for use as a buffer layer in between the electrolyte and electrode for solid oxide fuel cells.

In order to understand the influence of active site alteration on the catalytic behaviour of Ruddlesden-popper oxide, a series was synthesized by altering the amount of Sm and Sr using the SSR method. In order to understand the active site engineering more effectively, thin film was also synthesized by picking up the two best optimized samples. The electrocatalytic behaviour was studied for this series of Ruddlesden-popper perovskite. The structural, microstructural, electronic along with catalytic studies was performed by YGA, XRD, SEM, XPS and CV. It was found that moderate electroactivity can be achieved with an increase in active sites on miniaturization with the phase change.

Along with ORR, oxygen evolution reaction (OER) is also important for many electrochemical devices and Ruddlesden-popper perovskite has an ability to function like electrocatalyst for OER as well. Therefore, another series was synthesis from $\text{SmSrNiO}_{4-\delta}$ with doping on Lanthanum and Calcium on A-site by solid state route method and their catalytic behavior was studied especially for OER and also their suitability for energy storage application. It was observed that one of the compositions of this series has a large value of specific capacitance and double layer capacitance, making it suitable choice as the catalyst for OER and also shows its prominence for energy storage application as hybrid capacitor electrode.

It was observed that Nickel is playing the crucial role in the catalytic activity of all the sample synthesized till now. Therefore, in the last part of this research work, thin film of nickel oxide was synthesized by sol gel method by taking different number of depositions and the effect of pH was studied on their catalytic activity. In this regard, solution of three different

medium (acidic, neutral and alkaline) was chosen as electrolyte solution for catalytic studies. It was observed that a particular sample of synthesized thin films shows promising behaviour for electrocatalysis in two media.

The present thesis is divided into seven chapters and a brief description is given below:

Chapter 1 Provides introduction about fuel cell, as well as comprehensive review of the literature. This chapter describes the motivation of the research work, the background and fundamentals of fuel cell, the essential requirements of fuel cell components, the mechanism and kinetics for the cathode, the materials selection for cathode, the current scenario of nickelate-based perovskite and layered perovskite materials along with an overview of SmSrNiO_{4-δ} based on the systems. The main objective of the present work is also included in this chapter.

Chapter 2 Discusses various experimental techniques used for the present investigations. It represents the details of implemented experimental instruments, analysis techniques and various synthesis routes adopted to synthesize the samples. Solid-state reaction route, sol-gel, and pulse laser deposition techniques were discussed, which were used to synthesize the proposed systems. A detailed description of employed instruments such as TGA, DSC, XRD, SEM, TEM, XPS, and CV measurements, etc. along with the important analysis techniques like Rietveld Refinement analysis has also been discussed in this section.

Chapter 3 Ruddlesden–Popper structured layered perovskite, (SmSr)NiO_{4-δ}, was synthesized at different sintering temperatures using a solid-state reaction technique. Porous and dense microstructures were obtained at sintering temperatures of 1250 °C and 1425 °C, respectively. The influence of electrocatalysis on the structures of both surfaces was studied comprehensively. Post cyclic voltammetry structural studies show the presence of Ni–(OH)₂

and Ni–OOH species for the samples, respectively, suggesting that they undergo different oxygen reduction reaction mechanisms.

Chapter 4 The influence of compositional engineering via active site alternation on catalytic behaviour has been studied for the Ruddlesden–Popper-based system $\text{Sm}_{2-x}\text{Sr}_x\text{NiO}_{4-\delta}$. A phase change from orthorhombic ($x = 0.6$) to tetragonal ($x = 1.0$) in bulk $\text{Sm}_{2-x}\text{Sr}_x\text{NiO}_{4-\delta}$ is confirmed by Rietveld (XRD) analysis, thermogravimetric analysis (TGA) and X-ray photoelectron spectroscopy (XPS). To alter the active sites, we fabricated thin films for $x = 0.6$ and $x = 1.0$ using a pulsed laser deposition technique. The electrocatalytic behaviour has been studied in an environmentally friendly medium, i.e., a neutral medium ($\text{pH} = 7$), for both bulk and thin films, and parameters such as transient response, electrochemical reversibility and oxygen evolution reactivity are measured. The cyclic voltammetry curves suggest that electrochemical reversibility for thin films is governed by adsorption as opposed to the diffusion observed for bulk samples. Our investigation further suggests that moderate electroactivity can be achieved with an increase in active sites on miniaturization with the phase change.

Chapter 5 A series of Ruddlesden popper oxide materials $\text{Sm}_{1-x}\text{La}_x\text{Sr}_{1-x}\text{Ca}_x\text{NiO}_{4-\delta}$ ($x = 0.00, 0.05, 0.10, 0.15, \text{ and } 0.20$) were synthesized and their electrochemical behavior was investigated in 1M KOH alkaline solution. Phase formation in all the sample is confirmed through XRD. SEM depicts the porous morphology of all the samples. FTIR confirms the presence of -OOH and -OH groups in several compositions. The Cyclic voltammetry curve of $\text{Sm}_{0.90}\text{La}_{0.10}\text{Sr}_{0.90}\text{Ca}_{0.10}\text{NiO}_{4-\delta}$ and $\text{Sm}_{0.80}\text{La}_{0.20}\text{Sr}_{0.80}\text{Ca}_{0.20}\text{NiO}_{4-\delta}$ indicates the presence of the combination of both pseudo capacitance and electrochemical double layer capacitance in these two electrodes. However, only the sample $\text{Sm}_{0.90}\text{La}_{0.10}\text{Sr}_{0.90}\text{Ca}_{0.10}\text{NiO}_{4-\delta}$ satisfy the condition of general power law for pseudo capacitance. This material also shows the highest value of

specific capacitance (910.20 F/g) and electrochemical double layer capacitance (238.25 mF/cm²) among all the samples. XPS analysis reveals that oxidation states of the Nickel and Oxygen play a crucial role for the better electrochemical performance of the electrode.

Chapter 6 Thin films of Nickel oxide (NiO) was synthesized by using sol gel method through spin coating technique on silica substrate with different number of layers deposition of NiO. XRD confirms the cubic phase formation of thin films and SEM and AFM confirm the well deposition of thin films on substrate. The catalytic activity was investigated of two extreme samples for oxygen evolution reaction and oxygen reduction reaction in all three mediums i.e., acidic, neutral, and alkaline mediums. It was found that the sample with highest number of deposition layers shows its suitability for electrocatalysis in alkaline and acidic mediums.

Chapter 7 Concludes the outcomes of the research works of this thesis and also propose the future scope of the present investigations.